Inorganic Chemistry
Cite This: Inorg. Chem. 2018, 57, 9403−9411
Article
pubs.acs.org/IC

Quaternary Chalcogenide Semiconductors with 2D Structures: $Rb_2ZnBi_2Se_5$ and $Cs_6Cd_2Bi_8Te_{17}$

Jing Zhao,[†,‡] Shiqiang Hao,[§] Saiful M. Islam,[∥] Haijie Chen,[‡] Shulan Ma,[‡] Chris Wolverton,[§] and Mercouri G. Kanatzidis*[,‡]

[†]The Beijing Municipal Key Laboratory of New Energy Materials and Technologies, School of Materials Sciences and Engineering, University of Science and Technology Beijing, Beijing 100083, China

[‡]Department of Chemistry and [§]Department of Materials Science and Engineering, Northwestern University, Evanston, Illinois 60208, United States

[∥]Department of Chemistry, Physics and Atmospheric Sciences, Jackson State University, Jackson, Mississippi 39217, United States

Supporting Information

ABSTRACT: Two new layered compounds $Rb_2ZnBi_2Se_5$ and $Cs_6Cd_2Bi_8Te_{17}$ are described. $Rb_2ZnBi_2Se_5$ crystallizes in the orthorhombic space group *Pnma*, with lattice parameters of a = 15.6509(17) Å, b = 4.218(8) Å, and c = 18.653(3) Å. $Cs_6Cd_2Bi_8Te_{17}$ crystallizes in the monoclinic $C2/m$ space group, with a = 28.646(6) Å, b = 4.4634(9) Å, c = 21.164(4) Å, and β = 107.65(3)°. The two structures are different and composed of anionic layers which are formed by inter connecting of BiQ_6 octahedra (Q = Se or Te) and MQ_4 (M = Zn or Cd) tetrahedra. The space between the layers hosts alkali metal as counter cations. The rubidium atoms of $Rb_2ZnBi_2Se_5$ structure can be exchanged with other cations (Cd^{2+}, Pb^{2+} and Zn^{2+}) in aqueous solutions forming new phases. $Rb_2ZnBi_2Se_5$ is an *n*-type semiconductor and exhibits an indirect band gap energy of 1.0 eV. $Rb_2ZnBi_2Se_5$ is a congruently melting compound (mp ∼644 °C). The thermal conductivity of this semiconductor is very low with 0.38 $W \cdot m^{-1} \cdot K^{-1}$ at 873 K. Density functional theory (DFT) calculations suggest that the low lattice thermal conductivity of $Rb_2ZnBi_2Se_5$ is attributed to heavy Bi atom induced slow phonon velocities and large Gruneisen parameters especially in the a and c directions. The thermoelectric properties of $Rb_2ZnBi_2Se_5$ were characterized with the highest ZT value of ∼0.25 at 839 K.

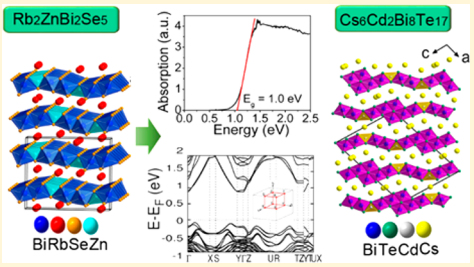

INTRODUCTION

Multinary bismuth chalcogenides exhibit some of the broadest structural and compositional diversity known in crystalline solids, which endows them with a wide range of physical properties such as thermoelectric, topological, superconductivity, and nonlinear optical properties.[1−6] Complex bismuth chalcogenides have a tendency to form low-dimensional structures, and many of which can be organized into homologous series. These include $A_m[M_{1+l}Se_{2+l}]_{2m}[M_{2l+n}Se_{2+3l+n}]$ (A = K, Rb, Cs, Sr, Ba; M = Bi, Sb, Pb, Sn),[7−9] $A_{1-x}M_{4-x}Bi_{11+x}Se_{21}$ (A = K, Rb, Cs; M = Sn, Pb),[7] $A_2[M_{5+n}Se_{9+n}]$ (A = Rb, Cs; M = Bi, Ag, Cd),[10] and $CsPb_mBi_3Te_{5+m}$.[11] The structures of selenides in these homologous series evolve systematically varying the size and shape of their NaCl- and Bi_2Se_3-type blocks, while the telluride compounds are built only from a single structural motif, a slice of NaCl-type block. The telluride series form layered structures that sandwich alkali metals, including $CsMBi_3Te_6$, $CsM_2Bi_3Te_7$ (M = Pb, Sn),[12,13] $CsM_3Bi_3Te_8$, $CsM_4Bi_3Te_9$ (M = Pb, Sn),[14] $CsBi_4Te_6$,[15,16] $RbBi_{3.67}Te_6$,[1] and $Cs_2Bi_{10}Q_{15}$ (Q = Se, Te).[17] The staggering compositional and structural diversity in bismuth chalcogenides derives from the $6s^2$ lone pair of electrons,[14,18] which can hybridize with p and d orbitals of Bi to generate sp^3d^2 octahedral coordination geometry or can localize to give distorted coordination.[19] This essentially allows Bi to adopt any coordination number from 3 to 7 or 8. The lone pair of the Bi^{3+} center also creates anharmonicity, which is beneficial to achieve very low thermal conductivities.[20−22] The structures of bismuth chalcogenides tend to share common fragments $[M_mQ_n]$ which are building blocks that derive from Bi_2Te_3-, Sb_2Se_3-, CdI_2-, or NaCl-type structures.[23,24] These blocks come in different shapes and sizes and connect to each other directly or via bridging units, e.g., ZnS_4, CdS_4, $CuSe_4$, or $SiSe_4$ tetrahedrons,[25−28] to form different structures.[29] A few representative examples of this class of compounds with bridging units are sulfides ABi_2CuS_4 (A = K, Cs),[27,30] $A_3Bi_5Cu_2S_{10}$ (A = K, Rb, Cs),[27,30] $CsBiAg_2S_3$,[20] $ABiMS_4$ (A = K, Rb, Cs; M = Si, Ge),[31,32] $Cs_4Cu_3Bi_9S_{17}$,[25] and $Cs_2MBi_2S_5$[28] (M = Cd, Zn, Mn). Corresponding chemistry with quaternary selenides is much less investigated, i.e., $RbBi_{2.66}CuSe_5$[30] and $Cs_2ZnBi_2Se_5$,[33] while no telluride examples have been reported.

Herein, we report two new layered compounds $Rb_2ZnBi_2Se_5$ and $Cs_6Cd_2Bi_8Te_{17}$. Here we show that ion exchange of the Rb^+ ions in $Rb_2ZnBi_2Se_5$ structure is possible with divalent

Received: May 22, 2018
Published: July 16, 2018

DOI: 10.1021/acs.inorgchem.8b01383
Inorg. Chem. 2018, 57, 9403−9411

cations generating new phases. $Cs_6Cd_2Bi_8Te_{17}$ features a unique 2D structure which is composed of $[CdBi_8Te_{17}]^{6-}$ layers separated by Cs^+ cations. $Rb_2ZnBi_2Se_5$, which has an isostructural Cs analog, is an indirect band gap semiconductor that exhibits an extremely low thermal conductivity (0.38 $W \cdot m^{-1} \cdot K^{-1}$ at 873 K). The origin of the low thermal conductivity was investigated with theoretical phonon and Gruneisen parameter calculations.

EXPERIMENTAL SECTION

Reagents. All chemicals were used as obtained: cadmium metal (99.9%, Strem Chemicals, Inc.), bismuth metal (99.9%, Strem Chemicals, Inc.), zinc metal (99.9%, Strem Chemicals, Inc.), selenium pellets (99.99%, American Elements, Inc.), tellurium metal (99.99%, Sigma-Aldrich, Inc.), and homemade Rb_2Se and Cs_2Te_3 which were obtained as described elsewhere.[34]

Synthesis. *$Rb_2ZnBi_2Se_5$.* $Rb_2ZnBi_2Se_5$ was synthesized by reacting a mixture of Rb_2Se (262.4 mg, 1.05 mmol), Bi (418 mg, 2.00 mmol), Zn (65.4 mg, 1.00 mmol), and Se (315.8 mg, 4.00 mmol). The reactants were loaded into a 9 mm carbon-coated fused-silica tube in a N_2 gas glovebox. The tube was taken out and flame-sealed under a vacuum of $\sim 10^{-4}$ mbar, and then heated from room temperature (RT) to 350 °C in 6 h and held for 6 h, then heated to 750 °C in 12 h and kept for 24 h, and subsequently cooled slowly to RT in 32 h. The obtained phase is pure as judged by powder X-ray diffraction (PXRD) and has barlike crystals with lengths up to millimeters. ***Caution**: Attempts to prepare 5 g/batch may result in explosion of the fused silica tube of 13 mm outer diameter according to the above heating profile, but amounts of ∼1 g can be prepared safely under similar experimental conditions.*

$Cs_6Cd_2Bi_8Te_{17}$. $Cs_6Cd_2Bi_8Te_{17}$ crystals were obtained by reacting a mixture of Cs_2Te_3 (194.6 mg, 0.30 mmol), Bi (167.2 mg, 0.80 mmol), Cd (22.5 mg, 0.20 mmol), and Te (102.1 mg, 0.80 mmol). The reactants were loaded into a 9 mm carbon-coated fused-silica tube in a glovebox which was filled with inert N_2 gas. The tube was taken out and flame-sealed at a vacuum of $\sim 10^{-4}$ mbar, then heated from RT to 350 °C in 6 h and held for 6 h for the complete melting of Te, then heated to 750 °C in 12 h and held for 18 h, followed by slow cooling to RT in 100 h. Barlike crystals of $Cs_6Cd_2Bi_8Te_{17}$ were obtained with length to a maximum of one millimeter. According to PXRD, the obtained $Cs_6Cd_2Bi_8Te_{17}$ is a minor phase with the major phase being $CsBi_4Te_6$.[35]

Powder X-ray Diffraction (PXRD). Rigaku Miniflex powder X-ray diffractometer with Ni-filtered Cu Kα radiation operating at 40 kV and 15 mA was used to examine the purity of the synthesized samples. Calculated PXRD pattern were generated by Mercury software using the CIFs of refined structures.

Scanning Electron Microscopy. Energy-dispersive X-ray spectroscopy (EDS) was performed by Hitachi S-3400 scanning electron microscope equipped with a PGT energy-dispersive X-ray analyzer, 25 kV accelerating voltage, 80 mA probe current, and 60 s acquisition time was used to get the spectrum. The results given here is an average of a large number of independent measurements.

Single Crystal X-ray Diffraction (SCXRD). STOE IPDS II single crystal diffractometer operating at 50 kV and 40 mA was used to conduct X-ray diffraction measurements with Mo Kα radiation (λ = 0.71073 Å). Single crystals of $Rb_2ZnBi_2Se_5$ and $Cs_6Cd_2Bi_8Te_{17}$ were picked up and adhered to the tips of glass fibers with glue. Data collections were carried out with X-Area software. X-RED and X-SHAPE are programs provided by STOE. X-RED was used to do the integration; X-SHAPE was used for numerical absorption corrections.[36] The crystal structures were solved by XPREP by using direct method and refined via the SHELXTL program package.[37] The atomic coordinates, equivalent isotropic displacement parameters, anisotropic displacement parameters, and selected bond lengths and bond angles of $Rb_2ZnBi_2Se_5$ are given in Tables S1−S3, and those of $Cs_6Cd_2Bi_8Te_{17}$ are given in Tables S4−S6.

Thermal Analysis. About 70 mg of $Rb_2ZnBi_2Se_5$ powder was placed into a carbon-coated fused silica ampule and then flame-sealed at a vacuum of $\sim 10^{-4}$ mbar. Shimadzu DTA-50 thermal analyzer was used to conduct the differential thermal analysis (DTA) measurement with a temperature rate of ±10 °C/min and a maximum temperature of 730 °C. The minimum of endothermic valleys and the maximum of exothermic peaks were denoted as melting and crystallization temperatures, respectively. The PXRD of the DTA product matches well with that taken from the sample before heating.

Infrared and Ultraviolet−Visible Spectroscopy. A Shimadzu UV-3600 PC double-beam, double-monochromator spectrophotometer was used to collect diffuse-reflectance spectra of $Rb_2ZnBi_2Se_5$. The instrument was equipped with an integrating sphere and controlled by a personal computer. $BaSO_4$ was served as a standard and set to 100% reflectance. The sample was ground into a fine powder and prepared by placing it on a bed of $BaSO_4$ in air. Collected reflectance data were converted to absorbance according to the Kubelka−Munk equation: $\alpha/S = (1 - R)^2/2R$, where R is reflectance, α is the absorption coefficient, and S is the scattering coefficient.[38−40] The absorption edge was estimated by linearly extrapolating the absorption edge against the energy axis.

Spark Plasma Sintering (SPS). The obtained $Rb_2ZnBi_2Se_5$ samples were crushed into fine powders and subsequently densified at 773 K, 10 min in a 12.7 mm diameter graphite die under an axial compressive stress of 40 MPa using SPS method (SPS-211LX, Fuji Electronic Industrial Co., Ltd.). A highly dense disc-shaped pellet with ∼93% of its theoretical density was obtained.

Electrical Properties. The $Rb_2ZnBi_2Se_5$ SPS-processed pellet was cut into bars perpendicular to the sintering pressure direction without contacting water. The samples were spray-coated with boron nitride to avoid outgassing while heating, except places needed for electrical contact. The Seebeck coefficients and electrical conductivities were measured in directions perpendicular to the sintering pressure with an Ulvac Riko ZEM-3 instrument simultaneously. The measurement was conducted under a low-pressure helium atmosphere with a temperature ranging from RT to 850 K. The uncertainty of the measurement is about 5%.[41]

Thermal Conductivity. The thermal diffusivity coefficients (D) were measured on samples cut from the same SPS-processed pellet using a Netzsch LFA457 instrument. The samples were coated with graphite in order to minimize errors arising from the emissivity of the material. The thermal diffusion was measured perpendicular to the sintering pressure direction and data analysis was conducted by the Cowan model with pulse correction.[42] The total thermal conductivity was obtained from the $\kappa_{tot} = DC_pd$ equation, where d is the actual density obtained by using the mass dividing the volume of the sample; the specific heat capacity (C_p) was calculated by the Dulong−Petit law $C_p = 3R/\bar{M}$, where R is the gas constant 8.314 $J \cdot mol^{-1} \cdot K^{-1}$ and $\bar{M}$ is the average molar mass. The uncertainty of the thermal conductivity and ZT is estimated to be ∼8 and 20% respectively.[41]

Density Functional Theory (DFT) Calculations. The total energies and relaxed geometries were calculated by DFT within the generalized gradient approximation (GGA) of Perdew−Burke−Ernzerhof the exchange correlation functional with Projector Augmented Wave potentials.[43] We used periodic boundary conditions and a plane wave basis set as implemented in the Vienna *ab initio* simulation package.[44] The total energies were numerically converged to approximately 3 meV/cation using a basis set energy cutoff of 500 eV and dense k-meshes corresponding to 4000 k-points per reciprocal atom in the Brillouin zone.

Phonon Dispersion Calculations. To quantitatively explore the origin of low lattice thermal conductivity at the atomic level, we employed the Debye−Callaway model to quantitatively evaluate the lattice thermal conductivity of $Rb_2ZnBi_2Se_5$.[45] It is known that the Grüneisen parameters, which characterize the relationship between phonon frequency and crystal volume change, allow us to estimate the lattice anharmonicity and better understand the physical nature of lattice thermal conductivity. The phonon and Grüneisen dispersions are calculated using first-principles DFT phonon calculations within the quasi-harmonic approximation. The $Rb_2ZnBi_2Se_5$ phonon dispersions are calculated on a 120 atom cell at two volumes: One

DOI: 10.1021/acs.inorgchem.8b01383
Inorg. Chem. 2018, 57, 9403−9411

is the equilibrium volume V_0, and the other is the isotropically compressed volume $0.985V_0$.

The Debye−Callaway formalism[46] has been shown to produce reasonably accurate values of lattice thermal conductivity, compared to those of experiment, for low-conductivity thermoelectric compounds.[45] The total lattice thermal conductivity can be written as a sum over one longitudinal κ_{LA} and two transverse κ_{TA} and $\kappa_{TA'}$ acoustic phonon branches: $\kappa_{Latt} = \kappa_{LA} + \kappa_{TA} + \kappa_{TA'}$. The partial conductivities κ_i (i corresponds to TA, TA′, and LA modes) are given by

$$\kappa_i = \frac{1}{3}C_i T^3 \left\{ \int_0^{\Theta_i/T} \frac{\tau_c^i(x) x^4 e^x}{(e^x-1)^2}\,dx + \frac{\left[\int_0^{\Theta_i/T} \frac{\tau_c^i(x) x^4 e^x}{\tau_N^i (e^x-1)^2}\,dx\right]^2}{\int_0^{\Theta_i/T} \frac{\tau_c^i(x) x^4 e^x}{\tau_N^i \tau_U^i (e^x-1)^2}\,dx} \right\} \quad (1)$$

In this expression, Θ_i is the longitudinal (transverse) Debye temperature, $1/\tau_N^i$ is the scattering rate for normal phonon processes, $1/\tau_R^i$ is the sum of all resistive scattering processes, and $1/\tau_c^i = 1/\tau_N^i + 1/\tau_R^i$, $x = \hbar\omega/k_B T$, and $C_i = k_B^4/2\pi^2\hbar^3 v_i$, where $\hbar$ is the Planck constant, k_B is the Boltzmann constant, ω is the phonon frequency, and v_i is the longitudinal or transverse acoustic phonon velocity.

In our case, the resistive scattering rate includes the scattering rates due to Umklapp phonon−phonon scattering ($1/\tau_U^i$) and normal phonon scattering ($1/\tau_N^i$). The normal phonon scattering and Umklapp can be written as

$$\frac{1}{\tau_N^{LA}(x)} = \frac{k_B^5 \gamma_{LA}^2 V}{M\hbar^4 v_{LA}^5} x^2 T^5 \quad (2)$$

$$\frac{1}{\tau_N^{TA/TA'}(x)} = \frac{k_B^5 \gamma_{TA/TA'}^2 V}{M\hbar^4 v_{TA/TA'}^5} x T^5 \quad (3)$$

$$\frac{1}{\tau_U^i(x)} = \frac{k_B^2 \gamma_i^2}{M\hbar v_i^2 \Theta_i} x^2 T^3 e^{-\theta_i/3T} \quad (4)$$

where γ, V, and M are the Gruneisen parameter, the volume per atom, and the average mass of an atom in the crystal, respectively. The Grüneisen parameter can be defined as $\gamma_i = -\frac{V\partial\omega_i}{\omega_i \partial V}$, characterizing the relationship between phonon frequency and volume change.

RESULTS AND DISCUSSION

Synthesis and Thermal Behavior. Single crystals of $Rb_2ZnBi_2Se_5$ were grown by slowly cooling (~22 °C/h) a stoichiometric mixture of the starting materials (~250 mg in total) from 750 °C in a vacuum-sealed fused silica tube. After optimizing the ratio of the starting materials, we found pure phase could be obtained with 5% excess Rb_2Se. The excess is needed to compensate for the loss of Rb_2Se via reaction with the silica tube wall (Figure 1a). The EDS elemental analysis on these rodlike crystals indicated a ratio of 2.1:0.9:1.9:5 for Rb/Zn/Bi/Se which is in good agreement with the crystallographic analysis (Figure S1a).

$Rb_2ZnBi_2Se_5$ is stable in air for weeks and slowly starts capturing moisture. DTA of the freshly prepared sample shows one endothermic peak at 644 °C that corresponds to the melting of $Rb_2ZnBi_2Se_5$ and an exothermic peak at 605 °C on cooling corresponding to recrystallization, Figure 1b. Recrystallization of $Rb_2ZnBi_2Se_5$ has been confirmed by PXRD measurement of the DTA product. No obvious change in PXRD pattern was observed after DTA suggesting the compound melts congruently, Figure S2.

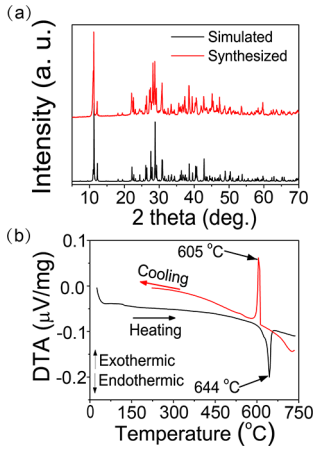

Figure 1. (a) Comparison of powder X-ray diffraction patterns of synthesized and simulated one of $Rb_2ZnBi_2Se_5$; (b) DTA curves of $Rb_2ZnBi_2Se_5$ reveal congruent melting behavior.

Single crystals of $Cs_6Cd_2Bi_8Te_{17}$ suitable for SCXRD were obtained with a reaction ratio of the elements as Cs/Cd/Bi/Te = 6:2:8:17. EDS on these needle-shaped crystals showed the presence of all four elements (Figure S1b). This material is difficult to obtain. Attempts to prepare the pure phase of $Cs_6Cd_2Bi_8Te_{17}$ using various experimental conditions and starting material ratios were unsuccessful because of the formation of thermodynamically more stable $CsBi_4Te_6$ as the main phase (confirmed by PXRD and EDS).[15−17] The inability to prepare pure phase restricted our efforts to conduct physical measurements on this material.

Structure Description. $Rb_2ZnBi_2Se_5$ crystallizes in the *Pnma* space group, and it is isostructural with $Cs_2ZnBi_2Se_5$[33] and $Cs_2ZnBi_2S_5$.[28] The unit cell parameters and refinement details of $Rb_2ZnBi_2Se_5$ are shown in Table 1. All atoms in the asymmetric cell are located on the *m* Wyckoff position. The crystal structure of $Rb_2ZnBi_2Se_5$ consists of $[ZnBi_2Se_5]^{2-}$ layers and Rb^+ cations located between the layers. There are two crystallographically independent Rb atoms: Rb1 is coordinated with six Se atoms forming distorted octahedra, whereas Rb2 is surrounded by seven Se atoms showing a monocapped trigonal prism coordination geometry (Figure 3). The Rb−Se distances range from 3.381(3) to 3.555(3) Å, which are comparable to those in $Rb_2Bi_8Se_{13}$.[47] There are two crystallographically distinct sites of Bi atoms, and both are in a distorted octahedral environment with bond distances ranging from 2.739(2) to 3.315(3) Å. There is only one type of tetrahedral Zn atom with bond lengths ranging from 2.457(3) to 2.525(4) Å, in agreement with that in $Cs_2Bi_2ZnSe_5$.[33] Two $[BiSe_6]$ octahedra are linked together by edge sharing to form binuclear bismuth fragments of $[Bi_2Se_{10}]$ which then propagate along the *b*-axis to form a ribbon. The ribbons are subsequently connected side by side in a parallel fashion by sharing corners to form corrugated layers. In these layers, Zn atoms are situated in tetrahedral sites (Figure 2). This structural characteristic of parallel ribbons can be linked to the bar like morphology of the crystals (Figure S1).

On the basis of these crystal structures, we performed DFT first-principles calculations on phase stability of $Rb_2ZnBi_2Se_5$ relative to their corresponding simple binary and ternary phases as listed in our Open Quantum Materials Database (OQMD).[48] We found the formation enthalpy of $Rb_2ZnBi_2Se_5$ (−0.787 eV/atom) is more favorable than those of the

DOI: 10.1021/acs.inorgchem.8b01383
Inorg. Chem. 2018, 57, 9403−9411

Table 1. Crystal Data and Structure Refinement for $Rb_2ZnBi_2Se_5$ and $Cs_6Cd_2Bi_8Te_{17}$ at 293(2) K[a]

fw	$Rb_2ZnBi_2Se_5$	$Cs_6Cd_2Bi_8Te_{17}$
cryst syst	orthorhombic	monoclinic
space group	*Pnma*	*C*2/*m*
unit cell dimensions	a = 15.6509(17) Å, b = 4.218(8) Å, c = 18.653(3) Å	a = 28.646(6) Å, b = 4.4634(9) Å, c = 21.164(4) Å, β = 107.65(3)°
V (Å^3)	1231(2)	2578.5(9)
Z	2	2
density (calcd) (g/cm^3)	5.659	6.264
abs coeff (mm^{-1})	53.020	41.602
F(000)	1760	3948
θ range for data collection (deg.)	2.82−29.15°	2.85−25.00°
index ranges	$-21 \le h \le 21$, $-5 \le k \le 5$, $-23 \le l \le 25$	$-34 \le h \le 34$, $-5 \le k \le 5$, $-25 \le l \le 25$
reflns collected	11440	8216
indep reflns	1863 [R_{int} = 0.0756]	2590 [R_{int} = 0.0794]
completeness to θ = 29.15°	99.1%	99.8%
refinement method	full-matrix least-squares on F^2	
data/restraints/params	1863/0/62	2590/0/106
GOF	0.947	1.003
final R indices [$>2\sigma(I)$]	R_1 = 0.0468, wR_1 = 0.1256	R_1 = 0.0494, wR_1 = 0.1052
R indices [all data]	R_2 = 0.0634, wR_2 = 0.1359	R_2 = 0.0723, wR_2 = 0.1137
largest diff. peak and hole (e·Å^{-3})	3.682 and −1.939	2.459 and −2.219

[a] $R = \Sigma||F_o| - |F_c||/\Sigma|F_o|$, $wR = \{\Sigma[w(|F_o|^2 - |F_c|^2)^2]/\Sigma[w(|F_o|^4)]\}^{1/2}$ and calcd $w = 1/[\sigma^2(F_o^2) + (0.1000P)^2 + 0.0000P]$ where $P = (F_o^2 + 2F_c^2)/3$ for $Rb_2ZnBi_2Se_5$ and $R = \Sigma||F_o| - |F_c||/\Sigma|F_o|$, $wR = \{\Sigma[w(|F_o|^2 - |F_c|^2)^2]/\Sigma[w(|F_o|^4)]\}^{1/2}$ and calcd $w = 1/[\sigma^2(F_o^2) + (0.0526P)^2 + 0.0000P]$ where $P = (F_o^2 + 2F_c^2)/3$ for $Cs_6Cd_2Bi_8Te_{17}$.

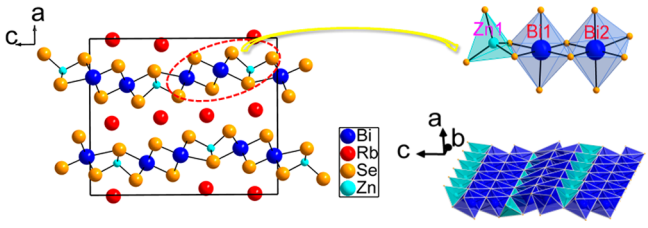

Figure 2. Unit cell of $Rb_2ZnBi_2Se_5$ and the $[ZnBi_2Se_5]$ layer.

respective phases of $Rb_2Bi_4Se_7$, ZnSe and Rb_3BiSe_3 by 38 meV/atom according to the grand canonical linear programming (GCLP) analysis.[49] The three simpler phases are selected with the most favorable energy based on GCLP algorithm. The calculated relative stability results support the experimental synthesis results.

$Cs_6Cd_2Bi_8Te_{17}$ is a new structure type that crystallizes in the monoclinic *C*2/*m* space group (Table 1). It possesses a 2D structure which is composed of $[CdBi_8Te_{17}]^{6-}$ layers separated by Cs^+ cations (Figure 4). All atoms in the unit cell occupy the *m* Wyckoff position, except Te6 and Cs1 which sit on the 2/*m* Wyckoff site. In the structure, the $[CdBi_8Te_{17}]$ slabs lie in an angle of 44.2 degrees relative to the *a*-axis. The Bi and Cd

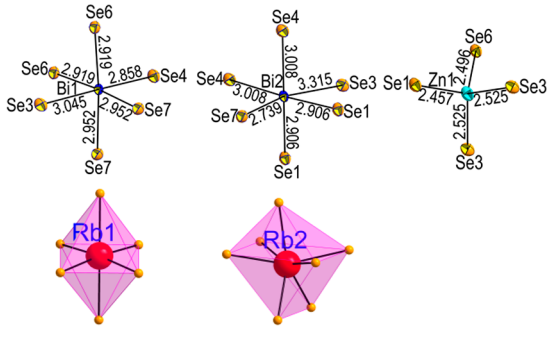

Figure 3. Atomic coordination environments of $Rb_2ZnBi_2Se_5$.

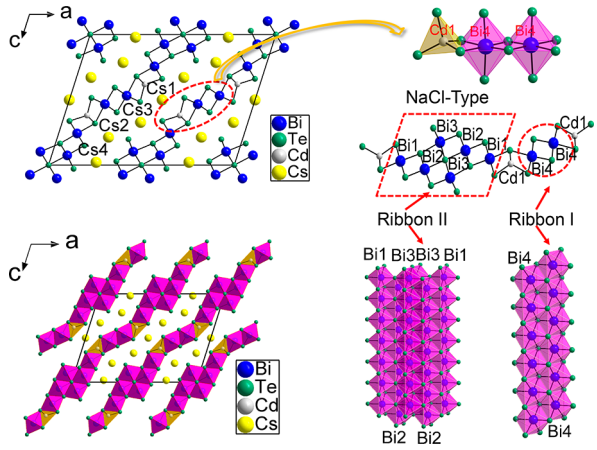

Figure 4. Unit cell of $Cs_6Cd_2Bi_8Te_{17}$ (top left), the layered $Cs_6Cd_2Bi_8Te_{17}$ viewing along different axis (down left) and the atomic construction details (right).

cation coordination environments are shown in Figure 5. There are four different types of Bi atoms, and all of them are

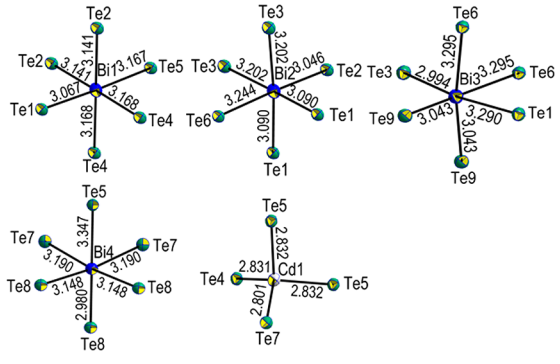

Figure 5. Atomic coordination environments of $Cs_6Cd_2Bi_8Te_{17}$.

DOI: 10.1021/acs.inorgchem.8b01383
Inorg. Chem. 2018, 57, 9403−9411

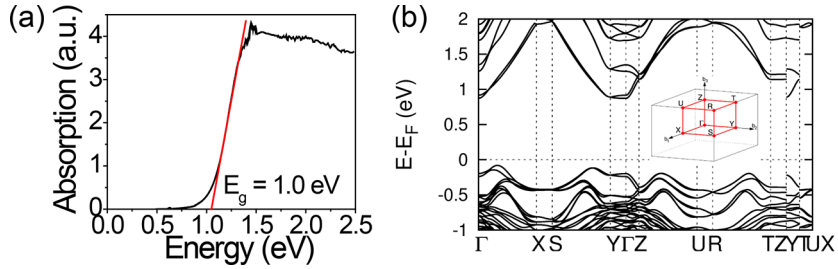

Figure 6. (a) UV−vis spectrum of $Rb_2ZnBi_2Se_5$ indicates a band gap of 1.0 eV and (b) Electronic band structures of $Rb_2ZnBi_2Se_5$. The inset figure is a Brillouin zone.

coordinated with six Te atoms forming distorted octahedral coordination geometries with bond lengths ranging from 2.980(2) to 3.347(2) Å, which is similar to those in $CsBi_4Te_6$ that adopts a very different crystal structure as discussed below.[16] Two $[Bi_4Te_6]$-based blocks connect together by edge sharing Te atoms forming a ribbon directing along *b*-axis (ribbon I), Figure 4. The Bi1, Bi2, and Bi3 octahedra are connected by edge sharing constituting a NaCl-type block, and viewing along *b*-axis, it forms a wider ribbon (ribbon II). There is only one type of Cd site which is coordinated with four Te atoms generating distorted tetrahedra with bond distances varying from 2.801(3) to 2.831(2) Å. The $CdTe_4$ serves as a bridge linking the two ribbons together by sharing edges to form a 2D slab. There are four crystallographically different Cs sites. The Cs4 site is half occupied by Cs atom. Figure 4 shows a polyhedral view of $Cs_6Cd_2Bi_8Te_{17}$ along *b* axis, which shows a corrugated layer parallel to the *b*-axis with Cs cations located in between.

The $Cs_6Cd_2Bi_8Te_{17}$ structure has some similarities with $CsBi_4Te_6$, with both of the structures composed of NaCl-type blocks forming two-dimensional layers with alkali metals residing between the layers. The difference is that the $CsBi_4Te_6$ structure is composed of nearly flat NaCl-type $[Bi_4Te_6]$ anionic layers and the $[Bi_4Te_6]$ layers themselves are made of parallel infinite rod shaped $[Bi_4Te_6]$ columns that are interconnected by characteristic Bi−Bi bonds with distance of 3.2383(10) Å.[15−17]

Ion Exchange Chemistry of $Rb_2ZnBi_2Se_5$. The alkali metals that reside between the layers of $Rb_2ZnBi_2Se_5$ can be exchanged with other cations in aqueous solution at room temperature which provides a facile low temperature route to prepare new and metastable compounds.[50] $Rb_2ZnBi_2Se_5$ crystals (∼10.0 mg) were immersed into 0.2 mol/L water solution (10 mL) of $ZnCl_2$, $CdCl_2$, and $Pb(NO_3)_2$ and were shaken for 24 h at RT; the solutions were then filtered and washed with water and acetone for several times. EDS of the solids after ion exchange showed that the divalent metal ions had entered into the structure and the Rb cations were totally removed (Figure S3).

After ion exchange, the band gaps of the samples decreased from 1.0 eV of the pristine one to 0.90 eV of Zn^{2+}, 0.88 eV of Cd^{2+}, and 0.61 eV of Pb^{2+} ion exchanged ones (Figure S4a). The narrowing of the bandgap with these divalent ions is in accordance with other reported results of compounds with similar ion exchange properties.[51,52] The products after ion exchange exhibit new Bragg peaks in PXRD with the main peaks of $Rb_2ZnBi_2Se_5$ becoming absent (Figure S4b). The PXRD could not be matched with any reported compounds suggesting new phases were synthesized. Therefore, we attempted to do the ion exchange in different time scales with the purpose of obtaining crystals good enough for single crystal XRD. Unfortunately, the crystals after ion exchange showed poor diffraction using our in-house X-ray sources and no unit cell parameters could be obtained. The characterization of these compounds is beyond the scope of this paper.

Optical Absorption and Electronic Structure. Electronic absorption spectrum measured on polycrystalline samples of $Rb_2ZnBi_2Se_5$ indicates a well-defined electronic absorption edge at 1.0 eV corresponding to the band gap (Figure 6a). First-principle electronic structure calculations indicate that $Rb_2ZnBi_2Se_5$ is an indirect band gap semiconductor with a band gap of 0.95 eV (Figure 6b). The indirect nature of the bandgap accounts for the sloping absorption edge which starts at 1.0 eV and ends at ∼1.4 eV. A noteworthy feature of the band structure is the rather broad nature conduction band which has positive implications for high electron mobilities. The projected electronic density of states, shown in Figure 7, indicate that the valence band

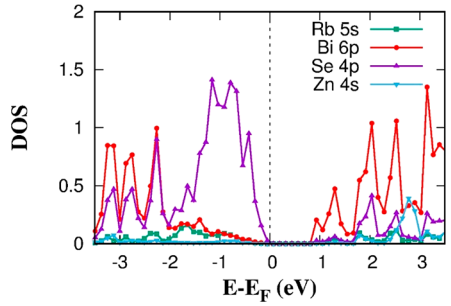

Figure 7. Projected electronic density of states of $Rb_2ZnBi_2Se_5$.

maximum is contributed mainly from Se 4p states and the conduction band minimum is from Bi 6p states. The contribution of Zn states in the conduction band minimum is negligible suggesting electron transport in this material is through Bi based 6p orbitals.

On the basis of the calculated band structure, we further evaluated the electron and hole effective mass of $Rb_2ZnBi_2Se_5$. The effective mass tensor m^* was calculated by $\frac{1}{m_{\alpha\beta}^*} = \frac{\partial^2 E}{\hbar^2 \partial k_\alpha k_\beta}$, where $\hbar$ is Plank's constant, E is the band energy, k is the wave vector, and α and β are directions. The density of states effective mass was then calculated as $m_{dos} = \sqrt[3]{m_{xx}^* m_{yy}^* m_{zz}^*}$. For electrons, the calculated effective masses are respectively $m_{xx} = 0.37m_0$, $m_{yy} = 4.96m_0$, $m_{zz} = 0.19m_0$, and $m_{dos} = 0.70m_0$, where m_0 is the effective mass of free electron. For holes, we consider two valence band maxima (VBM). The first VBM is along Γ−X, and the second is along S−Y. For the first VBM, the calculated effective mass are respectively $m_{xx} = 0.49m_0$, m_{yy} =

DOI: 10.1021/acs.inorgchem.8b01383
Inorg. Chem. 2018, 57, 9403−9411

$0.47m_0$, $m_{zz} = 2.94m_0$, and $m_{dos} = 0.88m_0$. For the second VBM, the calculated effective masses are respectively $m_{xx} = 0.72m_0$, $m_{yy} = 0.87\ m_0$, $m_{zz} = 6.58m_0$, and $m_{dos} = 1.60m_0$. These values confirm the anisotropic nature of the material and point to the intralayer directions as the most facile for charge transport.

Electrical and Thermal Transport Properties. For transport measurements polycrystalline samples of $Rb_2ZnBi_2Se_5$ were consolidated into strong pellets using SPS which were cut in the manner shown in Figure 8. The SEM

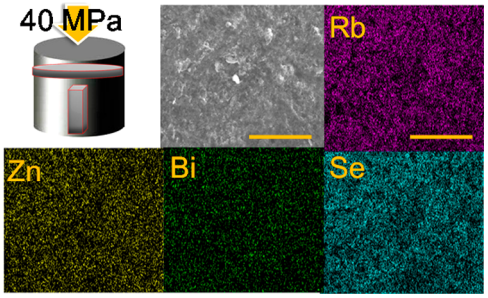

Figure 8. Samples cutting motif and pressure directions in the pellet processed by SPS; fresh surface of SPS-processed $Rb_2ZnBi_2Se_5$ sample characterized by SEM and energy-dispersive X-ray spectroscopy. The scale bar represents 100 μm.

image of fresh surface show that the samples are fully dense without noticeable cracks or pores and the EDS elemental maps of the imaged area indicate all elements are homogeneously dispersed.

The polycrystalline SPSed samples of $Rb_2ZnBi_2Se_5$ exhibits an electrical conductivity of 52 S·cm^{-1} at 323 K which decreases with increasing temperature to 30 S·cm^{-1} at 723 K followed by a small upturn to 37 S·cm^{-1} at 850 K (Figure 9a).

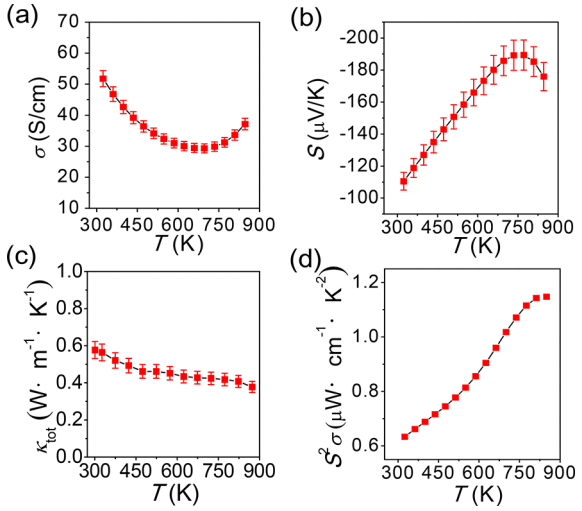

Figure 9. (a) Electrical conductivity, (b) Seebeck coefficient, (c) thermal conductivity, and (d) power factor values as a function of temperature for $Rb_2ZnBi_2Se_5$.

The Seebeck coefficients are negative in the entire temperature range, suggesting electrons as the majority carriers. The Seebeck values of $Rb_2ZnBi_2Se_5$ vary from −110.5 at RT to the maximum of −188.5 μV·K^{-1} at 723 K and then above that temperature decreases to −176 μV·K^{-1} at 850 K corresponding to the turn observed in the electrical conductivity (Figure 9b).

$Rb_2ZnBi_2Se_5$ possesses a very low thermal conductivity of ~0.58 W·m^{-1}·K^{-1} at 300 K which decreases to the lowest value of 0.38 W·m^{-1}·K^{-1} at 873 K (Figure 9c). The electronic contribution to the thermal conductivity is negligible given the low electrical conductivity (<52 S·cm^{-1}). The reversibility of all these measurements was good, as shown in Figure S5. The very low thermal conductivity of this material is at the same level of some state-of-the-art thermoelectric materials known for their ultralow thermal conductivities, i.e., $Cu_{2-x}Se$ (0.66–1.1 W·m^{-1}·K^{-1}),[53] $AgSbSe_2$ (0.23–0.4 W·m^{-1}·K^{-1}),[21] $CsAg_5Te_3$ (0.18–0.14 W·m^{-1}·K^{-1}),[54] $Cu_{2-x}S$ (0.25–0.6 W·m^{-1}·K^{-1}),[55] and Ag_9GaSe_6 (0.26–0.45 W·m^{-1}·K^{-1}),[56] and so on.

To understand the physical origin of this ultralow thermal conductivity, we performed DFT based phonon calculations (Figure 10). As shown in Figure 10d, the theoretically

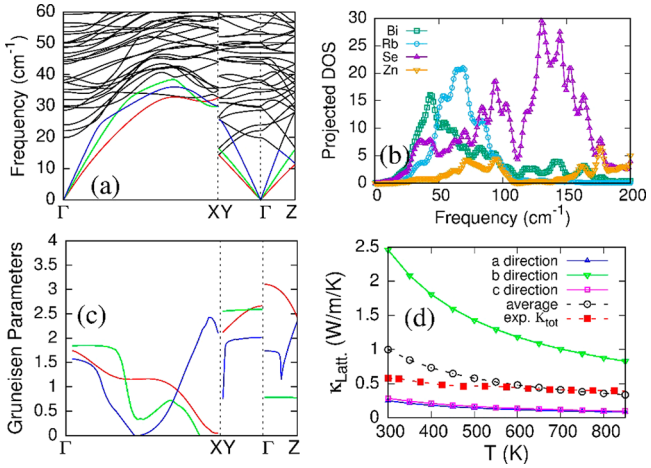

Figure 10. Calculated lattice dynamics of $Rb_2ZnBi_2Se_5$. (a) Phonon dispersion, (b) phonon density of states, (c) Gruneisen parameters, and (d) the calculated lattice thermal conductivities in three different lattice directions are shown in blue, green, and magenta. The arithmetic average lattice thermal conductivity values are plotted in black circles to compare with experimental total thermal conductivity shown in red squares.

calculated $Rb_2ZnBi_2Se_5$ lattice thermal conductivities along the *a* and *c* directions are so low as around 0.3 W·m^{-1}·K^{-1} at 300 K. For *b* (4.218 Å) direction, the relatively short lattice dimension than *a* (15.65 Å) and *c* (18.65 Å) induces relative larger Debye temperatures. The larger Debye temperature together with relative low Gruneisen parameters in the *b* direction in higher lattice thermal conductivity of 2.5 W·m^{-1}·K^{-1} at 300 K along the *b* direction. To compare the experimental polycrystalline observations, we consider the average of calculated lattice thermal conductivity over the three lattice directions based on the simple orthorhombic Brillouin zone. The average values are shown in black circles in Figure 10d, in which the near room temperature values are higher than the experimental results as red squares, but at high temperatures they agree well, as shown in Figure 10d. As can be seen, the calculated value of 1 W·m^{-1}·K^{-1} at 300 K gradually decreases to 0.4 W·m^{-1}·K^{-1} at 850 K. The higher average values than experimental lattice thermal conductivity near room temperature are attributed to the fact that we only consider acoustic phonon normal and Umklapp scattering processes for pure single crystal. Other phonon-scattering mechanisms present in real samples such as defects and grain

DOI: 10.1021/acs.inorgchem.8b01383
Inorg. Chem. 2018, 57, 9403–9411

boundary contributions are not accounted in our calculations. Physically, the averaged low lattice thermal conductivity is attributable to the very low phonon velocities along the *a* and *c* directions, which are both around 1600, 1920, and 2800 m/s for TA, TA′, and LA modes (Figure 10b). The low phonon velocities primarily originate from acoustic low-frequency vibrations from the heavier Bi atoms with minimal contribution from Zn. However, the highly anisotropic structure induces relatively large Gruneisen parameters in Γ−Y and Γ−Z directions hence very low lattice thermal conductivity in the *a* and *c* directions (Figure 10c).

The power factor (PF = $S^2\sigma$) of $Rb_2ZnBi_2Se_5$ ∼ 1.1 $\mu W \cdot cm^{-1} \cdot K^{-2}$ at 850 K is low and comparable to that of undoped $AgBi_3S_5$ (∼1.5 $\mu W \cdot cm^{-1} \cdot K^{-2}$ at 750 K; Figure 9d).[57] Nevertheless, because of the extremely low thermal conductivity $Rb_2ZnBi_2Se_5$ exhibits decent ZT value of 0.25 at 839 K, comparable to undoped $AgBi_3S_5$ of ∼0.22 at 750 K (Figure 11). After chlorine doping, $AgBi_3S_5$ was shown to achieve

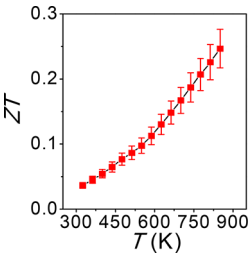

Figure 11. Figure of merit (ZT) values as a function of temperature for $Rb_2ZnBi_2Se_5$.

improved PF and a ZT of ∼1.0. Thus, we believe there is room for improvement in the ZT values of $Rb_2ZnBi_2Se_5$ by increasing the carrier concentration in the $[ZnBi_2Se_5]^{2-}$ network.[58]

CONCLUDING REMARKS

Two new chalcogenides $Rb_2ZnBi_2Se_5$ and $Cs_6Cd_2Bi_8Te_{17}$ with 2D structures were obtained. $Rb_2ZnBi_2Se_5$ is isostructural to $Cs_2ZnBi_2Se_5$, while $Cs_6Cd_2Bi_8Te_{17}$ possesses a new structure type. Both structures are formed by internal stacking of slabs that contain $BiSe_6$ octahedra and MSe_4 (M = Zn, Cd) tetrahedra. $Rb_2ZnBi_2Se_5$ is an *n*-type semiconductor with an indirect band gap of 1.0 eV. The alkali metals in $Rb_2ZnBi_2Se_5$ are loosely held in the structure and can be ion-exchanged with other cations at room temperature to form new phases. $Rb_2ZnBi_2Se_5$ possesses ultralow thermal conductivity with the lowest value of 0.38 $W \cdot m^{-1} \cdot K^{-1}$ at 873 K and which is in good agreement with theoretically calculated values, and in its undoped state, it exhibits a ZT value of ∼0.25 at 839 K.

ASSOCIATED CONTENT

Supporting Information

The Supporting Information is available free of charge on the ACS Publications website at DOI: 10.1021/acs.inorgchem.8b01383.

X-ray crystallographic data of $Rb_2ZnBi_2Se_5$ and $Cs_6Cd_2Bi_8Te_{17}$ in CIF format; Tables of atomic coordinates, displacement parameters, anisotropic displacement parameters and bond distances of $Rb_2ZnBi_2Se_5$ and $Cs_6Cd_2Bi_8Te_{17}$; SEM image and energy-dispersive X-ray spectroscopy spectrum of $Rb_2ZnBi_2Se_5$ and $Cs_6Cd_2Bi_8Te_{17}$; PXRD pattern of DTA product of $Rb_2ZnBi_2Se_5$; SEM images and Energy-dispersive X-ray spectroscopy spectra, optical absorption spectra and PXRD patterns of ion exchanged products of $Rb_2ZnBi_2Se_5$; thermal stability of electrical conductivity, Seebeck coefficients, and thermal diffusion coefficients of $Rb_2ZnBi_2Se_5$ (PDF)

Accession Codes

CCDC 1845892 and 1845971 contain the supplementary crystallographic data for this paper. These data can be obtained free of charge via www.ccdc.cam.ac.uk/data_request/cif, or by emailing data_request@ccdc.cam.ac.uk, or by contacting The Cambridge Crystallographic Data Centre, 12 Union Road, Cambridge CB2 1EZ, UK; fax: +44 1223 336033.

AUTHOR INFORMATION

Corresponding Author

*E-mail: m-kanatzidis@northwestern.edu.

ORCID

Jing Zhao: 0000-0002-8000-5973
Saiful M. Islam: 0000-0001-8518-1856
Haijie Chen: 0000-0003-3567-1763
Shulan Ma: 0000-0002-8326-3134
Chris Wolverton: 0000-0003-2248-474X
Mercouri G. Kanatzidis: 0000-0003-2037-4168

Notes

The authors declare no competing financial interest.

ACKNOWLEDGMENTS

This work was supported in part by Beijing Natural Science Foundation, China (2182080, 2182029) and a Grant from the National Science Foundation of China (51702329). At Northwestern this work was supported by the National Science Foundation (Grant DMR-1708254, exploratory synthesis and characterization). This work made use of the EPIC facility (NUANCE Center-Northwestern University), which has received support under the State of Illinois, Northwestern University, and the National Science Foundation with Grants DMR-1121262 through the MRSEC program at the Materials Research Center, and EEC-0118025/003 through The Nanoscale Science and Engineering Center. S. H. and C.W. (DFT calculations) acknowledge support from the Department of Energy, Office of Science Basic Energy Sciences under Grant DE-SC0014520. Access of QUEST, the supercomputer resources facilities at Northwestern University, is acknowledged.

REFERENCES

(1) Malliakas, C. D.; Chung, D. Y.; Claus, H.; Kanatzidis, M. G. Superconductivity in the narrow gap semiconductor $RbBi_{11/3}Te_6$. *J. Am. Chem. Soc.* **2016**, *138*, 14694−14698.

(2) Liu, Z.; Yao, X.; Shao, J.; Zuo, M.; Pi, L.; Tan, S.; Zhang, C.; Zhang, Y. Superconductivity with topological surface state in $Sr_xBi_2Se_3$. *J. Am. Chem. Soc.* **2015**, *137*, 10512−10515.

(3) Chung, I.; Song, J. H.; Jang, J. I.; Freeman, A. J.; Ketterson, J. B.; Kanatzidis, M. G. Flexible polar nanowires of $Cs_5BiP_4Se_{12}$ from weak interactions between coordination complexes: Strong nonlinear optical second harmonic generation. *J. Am. Chem. Soc.* **2009**, *131*, 2647−2656.

(4) Zhao, J.; Islam, S. M.; Hao, S.; Tan, G.; Su, X.; Chen, H.; Lin, W.; Li, R.; Wolverton, C.; Kanatzidis, M. G. Semiconducting

DOI: 10.1021/acs.inorgchem.8b01383
Inorg. Chem. 2018, 57, 9403−9411

pavonites $CdMBi_4Se_8$ (M = Sn and Pb) and their thermoelectric properties. *Chem. Mater.* **2017**, *29*, 8494−8503.
(5) Xu, B.; Feng, T.; Agne, M. T.; Zhou, L.; Ruan, X.; Snyder, G. J.; Wu, Y. Highly porous thermoelectric nanocomposites with low thermal conductivity and high figure of merit from large-scale solution-synthesized $Bi_2Te_{2.5}Se_{0.5}$ hollow nanostructures. *Angew. Chem.* **2017**, *129*, 3600.
(6) Zhang, H.; Liu, C.; Qi, X.; Dai, X.; Fang, Z.; Zhang, S. Topological insulators in Bi_2Se_3, Bi_2Te_3 and Sb_2Te_3 with a single Dirac cone on the surface. *Nat. Phys.* **2009**, *5*, 438−442.
(7) Mrotzek, A.; Chung, D. Y.; Ghelani, N.; Hogan, T.; Kanatzidis, M. G. Structure and thermoelectric properties of the new quaternary bismuth selenides $A_{1-x}M_{4-x}Bi_{11+x}Se_{21}$ (A = K and Rb and Cs; M = Sn and Pb) - Members of the grand homologous series $K_m(M_6Se_8)_m(M_{5+n}Se_{9+n})$. *Chem. - Eur. J.* **2001**, *7*, 1915−1926.
(8) Kanatzidis, M. G. Structural evolution and phase homologies for "design" and prediction of solid-state compounds. *Acc. Chem. Res.* **2005**, *38*, 359−368.
(9) Mrotzek, A.; Kanatzidis, M. G. "Design" in solid-state chemistry based on phase homologies. The concept of structural evolution and the new megaseries $A_m[M_{1+l}Se_{2+l}]_{2m}[M_{2l+n}Se_{2+3l+n}]$. *Acc. Chem. Res.* **2003**, *36*, 111−119.
(10) Kim, J. H.; Chung, D. Y.; Kanatzidis, M. G. A new chalcogenide homologous series $A_2[M_{5+n}Se_{9+n}]$(A = Rb, Cs; M = Bi, Ag, Cd). *Chem. Commun.* **2006**, *15*, 1628−1630.
(11) Guéguen, A.; Quarez, E.; Kanatzidis, M. G. Substitutions in the homologous family $CsPb_mBi_3Te_{5+m}$ and preliminary thermoelectric results. *MRS Online Proc. Libr.* **2005**, *886*, F08-06 DOI: 10.1557/PROC-0886-F08-06.
(12) Hsu, K. F.; Chung, D. Y.; Lal, S.; Mrotzek, A.; Kyratsi, T.; Hogan, T.; Kanatzidis, M. G. $CsMBi_3Te_6$ and $CsM_2Bi_3Te_7$ (M = Pb, Sn): New thermoelectric compounds with low-dimensional structures. *J. Am. Chem. Soc.* **2002**, *124*, 2410−2411.
(13) Malliakas, C. D.; Chung, D. Y.; Claus, H.; Kanatzidis, M. G. Superconductivity in the 2-dimensional homologous series AM_mBiQ_{5+m} (m = 1, 2) (A = Rb, Cs; M = Pb, Sn; Q = Se, Te). *Chem. - Eur. J.* **2018**, *24*, 7118−7122.
(14) Hsu, K. F.; Lal, S.; Hogan, T.; Kanatzidis, M. G. $CsPb_3Bi_3Te_8$ and $CsPb_4Bi_3Te_9$: low-dimensional compounds and the homologous series $CsPb_mBi_3Te_{5+m}$. *Chem. Commun.* **2002**, *13*, 1380−1381.
(15) Chung, D. Y.; Hogan, T.; Brazis, P.; Rocci-Lane, M.; Kannewurf, C.; Bastea, M.; Uher, C.; Kanatzidis, M. G. $CsBi_4Te_6$: A high-performance thermoelectric material for low-temperature applications. *Science* **2000**, *287*, 1024−1027.
(16) Chung, D. Y.; Hogan, T. P.; Rocci-Lane, M.; Brazis, P.; Ireland, J. R.; Kannewurf, C. R.; Bastea, M.; Uher, C.; Kanatzidis, M. G. A new thermoelectric material: $CsBi_4Te_6$. *J. Am. Chem. Soc.* **2004**, *126*, 6414−6428.
(17) Chung, D. Y.; Uher, C.; Kanatzidis, M. G. Sb and Se substitution in $CsBi_4Te_6$: the semiconductors CsM_4Q_6 (M = Bi, Sb; Q = Te, Se), $Cs_2Bi_{10}Q_{15}$, and $CsBi_5Q_8$. *Chem. Mater.* **2012**, *24*, 1854−1863.
(18) Chatterjee, A.; Biswas, K. Solution-based synthesis of layered intergrowth compounds of the homologous $Pb_mBi_{2n}Te_{3n+m}$ series as nanosheets. *Angew. Chem., Int. Ed.* **2015**, *54*, 5623−5627.
(19) Kyratsi, T.; Chung, D. Y.; Dyck, J. S.; Uher, C.; Lal, S.; Loo, S.; Hogan, T.; Ireland, J.; Kannewurf, C. R.; Hatzikraniotis, E.; Paraskevopoulos, K. M.; Kanatzidis, M. G. Synthesis, crystal structure and thermoelectric properties of β-$K_2Bi_8Se_{13}$ solid solutions. *MRS Online Proc. Libr.* **2003**, *793*, S9.2.
(20) Seshadri, R.; Hill, N. A. Visualizing the role of Bi 6s "Lone Pairs" in the off-center distortion in ferromagnetic $BiMnO_3$. *Chem. Mater.* **2001**, *13*, 2892−2899.
(21) Guin, S. N.; Chatterjee, A.; Negi, D. S.; Datta, R.; Biswas, K. High thermoelectric performance in tellurium free p-type $AgSbSe_2$. *Energy Environ. Sci.* **2013**, *6*, 2603−2608.
(22) Nielsen, M. D.; Ozolins, V.; Heremans, J. P. Lone pair electrons minimize lattice thermal conductivity. *Energy Environ. Sci.* **2013**, *6*, 570−578.
(23) Iordanidis, L.; Kanatzidis, M. G. Novel quaternary lanthanum bismuth sulfides $Pb_2La_xBi_{8-x}S_{14}$, $Sr_2La_xBi_{8-x}S_{14}$, and $Cs_2La_xBi_{10-x}S_{16}$ with complex structures. *Inorg. Chem.* **2001**, *40*, 1878−1887.
(24) Iordanidis, L.; Brazis, P. W.; Kannewurf, C. R.; Kanatzidis, M. G. Synthesis and thermoelectric properties of $Cs_2Bi_{7.33}Se_{12}$, $A_2Bi_8Se_{13}$ (A = Rb, Cs), $Ba_{4-x}Bi_{6+2/3x}Se_{13}$, and $Ba_{3\pm x}Pb_{3\pm x}Bi_6Se_{15}$. *MRS Online Proc. Libr.* **1998**, *545*, 189.
(25) Zhao, J.; Islam, S. M.; Tan, G. J.; Hao, S. Q.; Wolverton, C.; Li, R. K.; Kanatzidis, M. G. The new semiconductor $Cs_4Cu_3Bi_9S_{17}$. *Chem. Mater.* **2017**, *29*, 1744−1751.
(26) Mei, D. J.; Lin, Z. S.; Bai, L.; Yao, J. Y.; Fu, P. Z.; Wu, Y. C. $KBiMS_4$ (M = Si, Ge): Synthesis, structure, and electronic structure. *J. Solid State Chem.* **2010**, *183*, 1640−1644.
(27) Yang, Y.; Brazis, P.; Kannewurf, C. R.; Ibers, J. A. Structures and conductivities of the quaternary A/Bi/Cu/S phases KBi_2CuS_4 and $A_3Bi_5Cu_2S_{10}$ (A = Rb, Cs). *J. Solid State Chem.* **2000**, *155*, 243−249.
(28) Huang, F. Q.; Somers, R. C.; McFarland, A. D.; Van Duyne, R. P.; Ibers, J. A. Syntheses, structures, optical properties, and theoretical calculations of $Cs_2Bi_2ZnS_5$, $Cs_2Bi_2CdS_5$, and $Cs_2Bi_2MnS_5$. *J. Solid State Chem.* **2003**, *174*, 334−341.
(29) Choi, K. S.; Chung, D. Y.; Mrotzek, A.; Brazis, P.; Kannewurf, C. R.; Uher, C.; Chen, W.; Hogan, T.; Kanatzidis, M. G. Modular construction of $A_{1+x}M_{4-2x}M'_{7+x}Se_{15}$ (A = K, Rb; M = Pb, Sn; M′ = Bi, Sb): A new class of solid state quaternary thermoelectric compounds. *Chem. Mater.* **2001**, *13*, 756−764.
(30) Huang, F. Q.; Mitchell, K.; Ibers, J. A. Syntheses and structures of the quaternary alkali-metal bismuth coinage-metal chalcogenides $K_3Bi_5Cu_2S_{10}$, $CsBi_2CuS_4$, $RbBi_{2.66}CuSe_5$, and $CsBiAg_2S_3$. *J. Alloys Compd.* **2001**, *325*, 84−90.
(31) Yao, J.; Deng, B.; Ellis, D. E.; Ibers, J. A. New quaternary bismuth sulfides: syntheses, structures, and band structures of $AMBiS_4$ (A = Rb, Cs; M = Si, Ge). *Inorg. Chem.* **2002**, *41*, 7094−7099.
(32) Mei, D.; Lin, Z.; Bai, L.; Yao, J.; Fu, P.; Wu, Y. $KBiMS_4$ (M = Si, Ge): synthesis, structure, and electronic structure. *J. Solid State Chem.* **2010**, *183*, 1640−1644.
(33) Yao, J. Y.; Ibers, J. A. $Cs_2Bi_2ZnSe_5$. *Acta Crystallogr., Sect. E: Struct. Rep. Online* **2004**, *60*, i111−i113.
(34) Hanko, J. A.; Sayettat, J.; Jobic, S.; Brec, R.; Kanatzidis, M. G. $A_2CuP_3S_9$ (A = K, Rb), $Cs_2Cu_2P_2S_6$, and $K_3CuP_2S_7$: new phases from the dissolution of copper in molten polythiophosphate fluxes. *Chem. Mater.* **1998**, *10*, 3040−3049.
(35) Datta, A.; Nolas, G. S. Solution-based synthesis and low-temperature transport properties of $CsBi_4Te_6$. *ACS Appl. Mater. Interfaces* **2012**, *4*, 772−776.
(36) *X-area, X-red, and X-shape*; Cie & Stoe: Darmstadt, Germany, 1998.
(37) Sheldrick, G. A short history of SHELX. *Acta Crystallogr., Sect. A: Found. Crystallogr.* **2008**, *64*, 112−122.
(38) Mccarthy, T. J.; Ngeyi, S. P.; Liao, J. H.; Degroot, D. C.; Hogan, T.; Kannewurf, C. R.; Kanatzidis, M. G. Molten-salt synthesis and properties of 3 new solid-state ternary bismuth chalcogenides, .beta.-$CsBiS_2$, .gamma.-$CsBiS_2$, and $K_2Bi_8Se_{13}$. *Chem. Mater.* **1993**, *5*, 331−340.
(39) Liao, J. H.; Kanatzidis, M. G. Quaternary $Rb_2Cu_2SnS_4$, $A_2Cu_2Sn_2S_6$ (A = Na, K, Rb, Cs), $A_2Cu_2Sn_2Se_6$ (A = K, Rb), $K_2Au_2SnS_4$, and $K_2Au_2Sn_2S_6$ - syntheses, structures, and properties of new solid-state chalcogenides based on tetrahedral $[SnS_4]^{4-}$ units. *Chem. Mater.* **1993**, *5*, 1561−1569.
(40) Chondroudis, K.; McCarthy, T. J.; Kanatzidis, M. G. Chemistry in molten alkali metal polyselenophosphate fluxes. Influence of flux composition on dimensionality. Layers and chains in $APbPSe_4$, $A_4Pb(PSe_4)_2$ (A = Rb, Cs), and $K_4Eu(PSe_4)_2$. *Inorg. Chem.* **1996**, *35*, 840−844.
(41) de Boor, J.; Gupta, S.; Kolb, H.; Dasgupta, T.; Muller, E. Thermoelectric transport and microstructure of optimized $Mg_2Si_{0.8}Sn_{0.2}$. *J. Mater. Chem. C* **2015**, *3*, 10467−10475.
(42) Borup, K. A.; de Boor, J.; Wang, H.; Drymiotis, F.; Gascoin, F.; Shi, X.; Chen, L.; Fedorov, M. I.; Muller, E.; Iversen, B. B.; Snyder, G.

DOI: 10.1021/acs.inorgchem.8b01383
Inorg. Chem. 2018, 57, 9403−9411

J. Measuring thermoelectric transport properties of materials. *Energy Environ. Sci.* **2015**, *8*, 423−435.
(43) Perdew, J. P.; Burke, K.; Ernzerhof, M. Generalized gradient approximation made simple. *Phys. Rev. Lett.* **1996**, *77*, 3865−3868.
(44) Kresse, G.; Furthmüller, J. Efficient iterative schemes for ab initio total-energy calculations using a plane-wave basis set. *Phys. Rev. B: Condens. Matter Mater. Phys.* **1996**, *54*, 11169−11186.
(45) Morelli, D. T.; Heremans, J. P.; Slack, G. A. Estimation of the isotope effect on the lattice thermal conductivity of group IV and group III-V semiconductors. *Phys. Rev. B: Condens. Matter Mater. Phys.* **2002**, *66*, 195304.
(46) Asen-Palmer, M.; Bartkowski, K.; Gmelin, E.; Cardona, M.; Zhernov, A.; Inyushkin, A.; Taldenkov, A.; Ozhogin, V.; Itoh, K. M.; Haller, E. Thermal conductivity of germanium crystals with different isotopic compositions. *Phys. Rev. B: Condens. Matter Mater. Phys.* **1997**, *56*, 9431.
(47) Iordanidis, L.; Brazis, P. W.; Kyratsi, T.; Ireland, J.; Lane, M.; Kannewurf, C. R.; Chen, W.; Dyck, J. S.; Uher, C.; Ghelani, N. A.; Hogan, T.; Kanatzidis, M. G. $A_2Bi_8Se_{13}$ (A = Rb, Cs), $CsBi_{3.67}Se_6$, and $BaBi_2Se_4$: new ternary semiconducting bismuth selenides. *Chem. Mater.* **2001**, *13*, 622−633.
(48) Saal, J. E.; Kirklin, S.; Aykol, M.; Meredig, B.; Wolverton, C. Materials design and discovery with high-throughput density functional theory: the open quantum materials database (OQMD). *JOM* **2013**, *65*, 1501−1509.
(49) R. Akbarzadeh, A.; Ozoliņš, V.; Wolverton, C. First-principles determination of multicomponent hydride phase diagrams: application to the Li-Mg-N-H system. *Adv. Mater.* **2007**, *19*, 3233−3239.
(50) Clearfield, A. Role of ion exchange in solid-state chemistry. *Chem. Rev.* **1988**, *88*, 125−148.
(51) Zhao, J.; Islam, S. M.; Kontsevoi, O. Y.; Tan, G.; Stoumpos, C. C.; Chen, H.; Li, R. K.; Kanatzidis, M. G. The two-dimensional $A_xCd_xBi_{4-x}Q_6$ (A = K, Rb, Cs; Q = S, Se): direct bandgap semiconductors and ion-exchange materials. *J. Am. Chem. Soc.* **2017**, *139*, 6978−6987.
(52) Zhao, J.; Islam, S. M.; Hao, S.; Tan, G.; Stoumpos, C. C.; Wolverton, C.; Chen, H.; Luo, Z.; Li, R.; Kanatzidis, M. G. Homologous series of 2D chalcogenides Cs-Ag-Bi-Q (Q = S, Se) with ion-exchange properties. *J. Am. Chem. Soc.* **2017**, *139*, 12601−12609.
(53) Liu, H.; Shi, X.; Xu, F.; Zhang, L.; Zhang, W.; Chen, L.; Li, Q.; Uher, C.; Day, T.; Snyder, G. J. Copper ion liquid-like thermoelectrics. *Nat. Mater.* **2012**, *11*, 422−425.
(54) Lin, H.; Tan, G.; Shen, J. N.; Hao, S.; Wu, L. M.; Calta, N.; Malliakas, C.; Wang, S.; Uher, C.; Wolverton, C.; et al. Concerted rattling in $CsAg_5Te_3$ leading to ultralow thermal conductivity and high thermoelectric performance. *Angew. Chem., Int. Ed.* **2016**, *55*, 11431−11436.
(55) He, Y.; Day, T.; Zhang, T.; Liu, H.; Shi, X.; Chen, L.; Snyder, G. J. High thermoelectric performance in non-toxic earth-abundant copper sulfide. *Adv. Mater.* **2014**, *26*, 3974−3978.
(56) Jiang, B.; Qiu, P.; Chen, H.; Zhang, Q.; Zhao, K.; Ren, D.; Shi, X.; Chen, L. An argyrodite-type Ag_9GaSe_6 liquid-like material with ultralow thermal conductivity and high thermoelectric performance. *Chem. Commun.* **2017**, *53*, 11658−11661.
(57) Tan, G.; Hao, S.; Zhao, J.; Wolverton, C.; Kanatzidis, M. G. High thermoelectric performance in electron-doped $AgBi_3S_5$ with ultralow thermal conductivity. *J. Am. Chem. Soc.* **2017**, *139*, 6467−6473.
(58) Biswas, K.; He, J.; Blum, I. D.; Wu, C. I.; Hogan, T. P.; Seidman, D. N.; Dravid, V. P.; Kanatzidis, M. G. High-performance bulk thermoelectrics with all-scale hierarchical architectures. *Nature* **2012**, *489*, 414−418.

DOI: 10.1021/acs.inorgchem.8b01383
Inorg. Chem. 2018, 57, 9403−9411